INNOVATIVE SIMULATION OF Al_2O_3 NANOFLUID HEAT TRANSFER USING ADVANCED MACHINE LEARNING METHODS

by

Carlos SERRANO [*]***, Edwin JACOME, Edwin POZO, Santiago CHOTO, Patricio ABARCA, and Jorge BUNAY***

Facultad de Mecánica, Escuela Superior Politécnica de Chimborazo (ESPOCH), Riobamba, Ecuador

Original scientific paper
https://doi.org/10.2298/TSCI230310006S

In both turbulent and laminar pipe flows, we were able to accurately forecast the beginning range of the convective thermal transferring coefficients of Al_2O_3 magnetized nanofluids using machine learning approaches. The simulations utilized two machine learning techniques: radial basis function-backpropagation (RB) and multiple linear regression analysis. First, we used multiple linear regression analysis to fit the polynomial equation. Afterwards, grid search cross-validation was employed to determine the optimal RB model with six hidden layer neurons. To evaluate the RB model, we compared numerical patterns of the parameters used to measure accuracy. The regression coefficient and mean square error were the most commonly utilized parameters in Reynolds number mass percentage simulations, R^2. In the case of a laminar flow, these numbers were found to be 0.99994 and 0.34, respectively. Additionally, the results for laminar flow conditions using Reynolds number-magnetic field strength simplification were ideal, with an mean square error of 3.85 and an R^2 value of 0.99993. By comparing the predicted values with the experimental results visually using 3-D smoothed surface plots, we were able to further prove that the model was valid and accurate. These revolutionary findings could spark new developments and encourage substantial improvements in nanotechnology and machine intelligence. These findings are an important asset for driving future research and development, which in turn makes significant contributions to the ever-expanding frontiers of these innovative fields.

Key words: *Al_2O_3, nanofluids, heat transfer, mean square error, Reynolds number, multiple linear regression*

Introduction

The suspension of nanoparticles in a base fluid produces nanofluids, a hybrid type of fluid [1, 2]. The nanoparticles can be in the form of metals and carbides to ceramics and others. Nanofluids have far better thermal characteristics and far less agglomeration than traditional heat transfer fluids like water or glycol, according to the research [3, 4]. Nanoparticles' larger surface areas allow them to interact with the fluid around them more strongly, which improves the nanofluid medium's dispersion and stability. In addition, the nanofluid's thermal characteristics are enhanced since the increased surface area allows for more efficient heat transmission processes. Significant implications for a range of scientific and technical applications are presented by these discoveries, which highlight the critical role of nanoparticle surface area in

[*] Corresponding author, e-mail: carlos.serrano@espoch.edu.ec

affecting nanofluid behavior and performance [5, 6]. Nanofluids have numerous applications due to their exceptional thermophysical features, which include heat exchange devices, energy systems, and solar heating.

One kind of nanofluid that stands out from the many is magnetic nanofluids (MNF) [7]. A base liquid can be used to disperse superparamagnetic nanoparticles, resulting in the formation of these unique nanofluids [8]. Materials containing such nanoparticles include magnetite (Al_2O_3) and oxides of metals (cobalt, iron, nickel, and nickel, to name a few) [9]. In addition, a magnetic field can alter the internal particle distribution's structural properties in a MNF. The diffusion coefficient, thermal conductivity, viscosity, and strength of the applied magnetic field are all thermal performance factors of the MNF that are affected by this. This transition turns the MNF into an extraordinary heat transfer medium that can be *controlled*, opening up exciting possibilities for thermal management and better heat transfer. So, several studies have examined MNF to assess their nanofluid-flow and heat transfer properties. In an experiment conducted by authors [7, 10], the convective heat transfer (CHT) coefficient was found to increase by approximately 40.79% and 58.19%, respectively, when an external magnetic field was applied to Al_2O_3 nanofluids. Four magnets placed outside the device generated the magnetic field. Additionally, the conditional nanofluids were evaluated in the absence of a magnetic field, while the base fluid was left unattended. The authors found that when Al_2O_3-water nanofluids were exposed to a 415 Gauss uniform gradient magnetic field, their CHT coefficient increased by 9.16%. Laminar CHT coefficients in ferro magnetized fluids with concentrations between 1.25% and 2.5% were measured under both persistent and irregular magnetic field conditions, and the authors discovered a difference of at least 19.8%.

Due to the large number of tests and the complications in structure the experiment lay-out, an accurate depiction of the magnetic field's activity has not been achieved. However, machine learning (ML) approaches provide a strong alternative, and MNF can be controlled, so it has a significant impact on the thermal conductivity of the base fluid. The ML-based stability and thermophysical property prediction for nanofluids is similarly in its infancy. The most fundamental metrics such as nanocomposite mass, average particle size, concentration, and nanofluid temperature could only be captured by ML models prior to the development of magnetic fields. Due to this, the present study used a novel ML strategy to simulate the CHT of Al_2O_3 nanofluids in a magnetic field. In order to generate enough experimental data for modelling and prediction, three ML methods – backpropagation (RB), multiple linear regession (MLR) analysis, and LSTM – were employed. High accuracy and wide application are anticipated outcomes of this study's thorough comparison of ML prediction results. Potentially, it might serve as a benchmark for handling smaller data models in the future.

Experimental methodology

Fabrication

The Al_2O_3-water nanofluids were produced using a widely used two-step technique. It all starts with getting your hands on some nanoparticles. The next thing to do is to mix the nanoparticles with the base liquid. Last but not least, dispersants were added to the nanofluids to maintain a stable suspension. For the studies, the generated nanofluid samples were tailored with nanoparticle mass percentages of 0.6 wt.%, 1.2 wt.%, 1.8 wt.%, and 2.4 wt.%, respectively. To improve nanoparticle dispersion and drastically decrease nanoparticle deposition, the dispersant tetramethylammonium hydroxide (TMAH) was included [11]. After weighing the Al_2O_3 nanoparticles and adding them to the same quantity of deionized water, the next step in preparation was to add the dispersion TMAH, which had the same weight as the nanoparticles. After dispersing the nanofluids, each sample underwent 90 minutes of ultrasonic stirring and 30 minutes of magnetic swirling to increase stability. The state diagrams for 10 minutes, 2 days, 5 days, 7 days, and 14 days show that the nanofluids were able to stay in a stable state throughout the experiment.

Experimentation on heat transfer

Figure 1 shows that the experiment stage's storing container was filled uniformly with the created nanofluids. The whole set of experimental tools included a data collecting end, circulating pipe-line spherical regulating valve, storage tank, floating tubular flow metre for liquids, and water pump. By setting up a data collection area, a heat dissipation section, and an experimental test section on the experimental stage, we made sure the flow circulation system would work smoothly. The experimental portion was a 14 mm diameter, 500 mm long, and 2 mm thick copper tube with a 150 W aluminum foil heating sheet wrapped evenly around its perimeter. By manipulating the temperature of the aluminum frustrate sheet and allowing the alumina nanofluids moving through the tube to convectively exchange heat with it, the heating power may be adjusted to meet the experimental need.

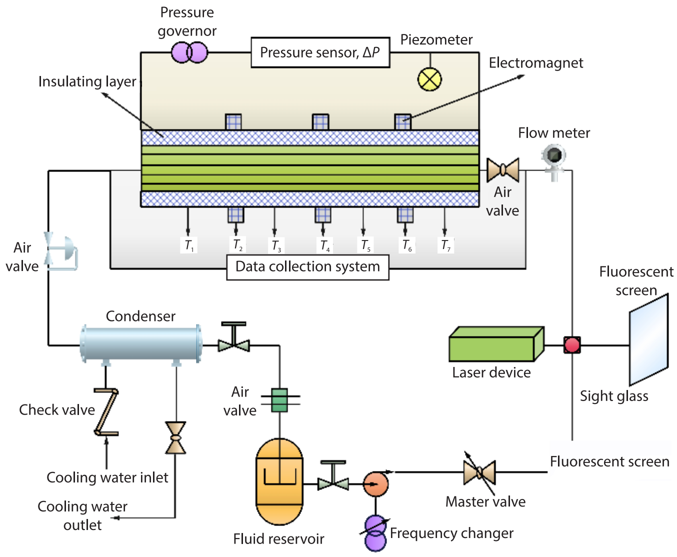

Figure 1. The Al_2O_3-water nanofluids experimental process

To reduce heat loss, the outside of the heating tube was covered with a uniform coating of insulating cotton. The water intake rate of the Al_2O_3-MNF can reach 15000 Lph due to a valve-controlled pump. Data collectors in the test area were linked to 7*T*-type thermocouples so that data could be captured in real-time. For the intake and exit measurements, separate *K*-type thermocouples were utilised. Using Nd2Fe14B permanent magnets attached to the T2/T4/T6 thermocouples at each of the six places outside the tube, a GM-2A Gauss metre was employed to ascertain the intensity of the vertical magnetic field. Flow metres, recording manometers, and other data collecting equipment were used to acquire experimental data, and the flow rate was controlled in the testing by adjusting the valves. Further assurance of the results' accuracy came from collecting experimental data three times using the same test parameters in order to take an average.

Verification of experimental system

In this part, we confirmed the stability and dependability of the test bench after successfully preparing the nanofluids and verifying the stabilisation. Initial experiments using deionized water's heat transfer characteristics in both laminar and turbulent flows determined that 2300 was the dividing line between the two. To compare the measured Nusselt number with authors [12], the Sieder and Dnielinski model was employed, which can be found in equations, whereas η is the viscosity of fluid and Pr indicates Prandtl number. Both models have been fitted to experimental data extensively and are applicable to many heat transport situations. They make it easier to gauge the efficacy of CHT by providing an estimate of the Nusselt number:

$$\mathrm{Nu} = 0.027\mathrm{Re}_f^{0.8}\mathrm{Pr}_f^{1/3}\left(\frac{\eta_f}{\eta_w}\right)^{0.14} \tag{1}$$

$$\mathrm{Nu} = 0.3 + \frac{\left(0.62\mathrm{Re}_f^{0.5}\mathrm{Pr}_f^{1/3}\right)}{\left[1+\left(\frac{0.4}{\mathrm{Pr}_f}0\right)^{2/3}\right]^{0.25}} \tag{2}$$

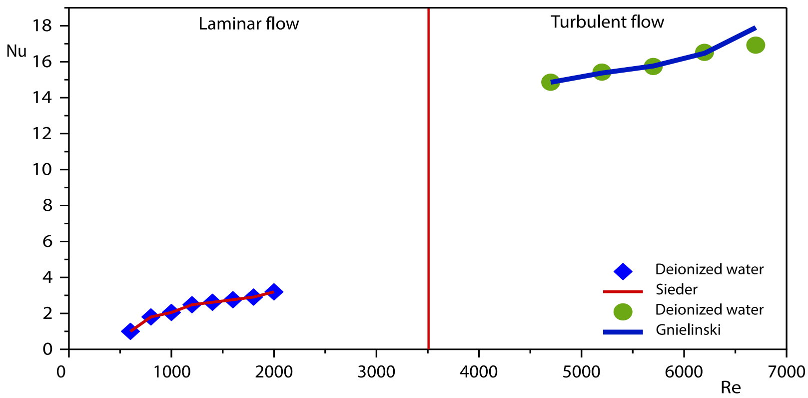

Figure 2. The flow chart for deionized water on the CHT process for verification purposes

The results, as shown in fig. 2, provide important and informative insights that enhance our comprehension of the study. The impressive CHT behaviour of MNF under laminar flow conditions can be predicted with high confidence by using the Sieder model, as shown by the excellent agreement between the model and the empirical observations, fig. 2. In the turbulent flow condition, the data strongly agree with the Dnielinski model, fig. 2, demonstrating that the model correctly depicts the CHT properties of MNF in this regime. This study's CHT test system was proven to be both suitable and effective by the robustness of these findings. The ability to reliably produce precise data shows that it could be a useful tool for studying convective heat transport in MNF, particularly when a magnetic field, B, is introduced.

The machine learning techniques

Search grid cross-validation

One of the most important factors in a ML model's performance is its hyperparameters [13]. Key hyperparameters of an ANN are the amount of hidden layers and the density of neurons per layer. To achieve the best possible model performance, it is crucial to choose these hyperparameters correctly. in the event that the hyper-parameters are not chosen appropriately, the model may end up being under- or overfitted [14]. To find the optimal combination of hyperparameters, one can use empirical fine-tuning, or one can systematically evaluate different parameter sizes. The latter method relies on human debugging, which can be laborious and lead to less-than-ideal selection of hyperparameters. Using grid search for cross-validation is the best way to fix this. Grid search iteratively trains the model and changes hyperparameters to discover the best combination that maximises accuracy by methodically exploring a predetermined parameter space.

Using assessment metrics derived from both the training and test sets, this work employs grid analyze with cross-validation (grid search CV) to determine the optimal parameters and neuronal density. All models are subjected to 20 iterations to guarantee robustness, and we showcase solely the model with the highest quality result. The effect of unpredictability on the developed models' performance is reduced by this method.

Multiple linear regression technique

Multiple linear regression analysis, in contrast to univariate linear regression, is applicable to a far wider variety of contexts as a model for assessing the relationship among variables. This is due, in large part, to the fact that, in contrast to real-world application scenarios, multivariate linear regression typically involves more than one independent variable [15]. That is, multiple linear regression analysis encompasses a wider range of scenarios and data points than a single independent variable analysis would. To express multiple linear regression, *Y*, mathematically, one can use the statement [16]:

$$Y = \beta_0 + \beta_1 X_1 + \beta_2 X_2 + \cdots + \beta_m X_m \tag{3}$$

To find the CHT coefficient, we use the following PYTHON-CODED and demonstrated procedures: analysis, regression, linearity, and using the Reynolds number, mass percentage, and MNF intensity of the Al_2O_3 in the pipe as independent variables.

Radial basis function-backpropagation technique

The primary and most significant obstacle is the development of an ANN capable of performing functions typically handled by the human central nervous system. [17]. Pattern recognition, data processing, process analysis, and ANN – a non-linear mathematical technique with learning capability, find extensive use. With their simple and easily implementable learning principles, neural networks are able to map arbitrary complex non-linear relationships, and their high non-linear fitting ability makes them ideal for computer implementations [18].

Typically, the ANN model in this analysis is depend on the backpropagating algorithm, which was first proposed in 1986 by a group of academics led by Rumelhart and Hinton [19]. Because of their superior multidimensional function mapping skills and their capacity to identify patterns of arbitrary complexity, backpropagating neural networks can tackle a wide variety of tasks, even many that simple perceptrons cannot. The number of training sessions can be reduced while improving prediction accuracy by intentionally combining the benefits of radial basis function (RBF) and backpropagating neural networks while backpropagating neural networks offer superior sample prediction, RBF neural networks can non-linearly approximatively handle any data collection. In fact, RB neural network architecture consists of two hidden layers. Both the RBF and backpropagating neural networks accomplish the same goal – the implementation of a hidden layer [20]. The three-layer architecture of the RB neural network utilised in the publication is illustrated in fig. 3. A stack consists of an input layer, a hidden layer, and an output layer. The data was divided into a training set with 70% of the total and a prediction set with 30% using PYTHON for neural network code creation and analysis. After that, six hidden layers were built from the data using the following properties as inputs: Reynolds number, mass percentage of Al_2O_3-MNF in the pipe, and magnetic field intensity. The CHT coefficient was the output parameter used for this prediction.

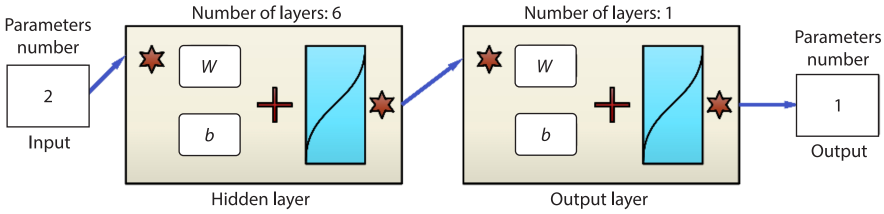

Figure 3. Network architecture of the RB layer

Results and discussion

Investigation of the factors impacting coefficient of CHT

The interfacial layer effect is a well-known explanation for the better enhancement of heat conductivity in nanofluids with a higher mass concentration of particles. The MNF test bench was utilised to examine the correlation between MNF concentration and its CHT coefficient in this case. Figure 4 displays the correlation between the Reynolds number and the CHT coefficient for MNF with variant particle masses, beginning at 40 °C and using a magnetic field of B = 850 G. Figure 4(a) demonstrates that, under laminar flow circumstances, the CHT coefficient increases exponentially with particle number for lower Reynolds numbers. Non-etheless, the values of the coefficient are nearly identical for particle concentrations of 2.4% and 1.8%. Particle mass concentrations of 0.6 %, 1.2 %, 1.8 %, and 2.4 % all resulted in CHT coefficient improvements of 0.88%, 1.56%, 2.14%, and 2.61%, respectively, at Reynolds number 1200. The CHT coefficients showed the most significant gains at Reynolds number 2000, with increases of 3.98%, 7.95%, 8.29%, and 8.74%, respectively, for the same mass concentrations. The results demonstrate that the CHT coefficient is greatly enhanced as the concentrations of nanofluids increase.

Figure 4(b) shows that there is a clear positive link between the Reynolds number and the CHT coefficient. The five curves also demonstrate that there is a flattening out of the curves until the Reynolds number reaches 5500, and then there is an insignificant rise beyond that. When the mass concentration hits 0.6% at a Reynolds number of 5500, the CHT coefficient of MNF increases by 2.12% related to deionized water. It would appear, though, that convective heat transmission in the tube does not have an immediately apparent enhancing impact. Specifically, the CHT coefficient goes up from 2.15% to 3.55%, 3.55%, and 5.55% when the mass concentration goes from 0.6% to 1.2% to 2.4%. The CHT coefficients of MNF with concentrations increases from 0.6% to 2.4% in deionized water were determined at 40 °C, with B = 850 G and a Reynolds number of 7500. The coefficients for these variables are 8260 W/m^{2}K, 8320 W/m^{2}K, 8540 W/m^{2}K, and 8760 W/m^{2}K, in that order. The production of nanoparticles with longer and more chain-like structures is induced by an increase in the concentration of MNF. This, in turn, enhances the heat transfer performance, which further improves the CHT coefficient. Moreover, as mentioned earlier, studies have demonstrated that

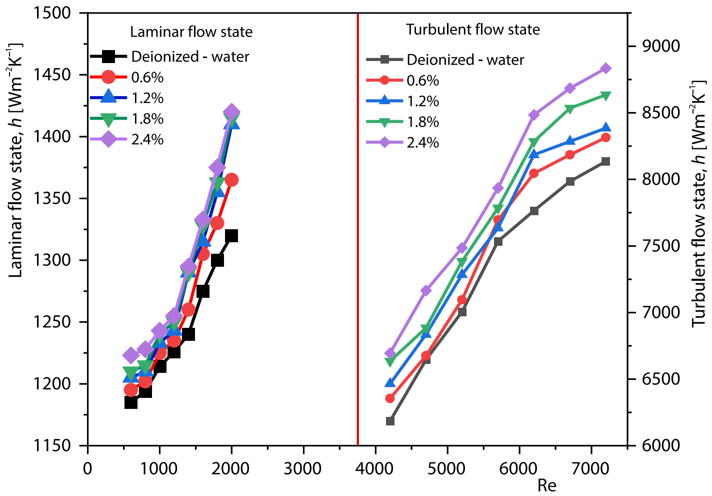

Figure 4. The relation among the CHT of Al_2O_3-water nanofluids and their mass percentage

thermal conductivity is improved by encasing nanoparticles in nanolayers [21]. This improvement is especially notable when considering the transitional thermal resistance between the solid and liquid phases. For MNF values between 0.6% and 2.4%, the CHT coefficient increases as concentration increases, following the increased thermal conductivity law.

Following this investigation, researchers continued to look into the crucial element of the applied magnetic field. At a tube temperature of 40 °C and a vertical magnetic field of B = 0 G, 250 G, 350 G, 650 G, 850G, and 1050 G, With a particle mass percentage of 1.2%, MNF provides tendency plots in fig. 5. The Reynolds number and CHT coefficient are positively correlated in both graphs. Similar to fig. 5(a), the CHT coefficient increases at B = 0 G and 250 G, and the plots overlap at 650 G, 850 G, and 1050 G. It may be inferred from this that, regardless of the strength of the magnetic field, there exists a critical value beyond which the field has no further effect on the rates of heat transfer coefficient increase. Under the same con-

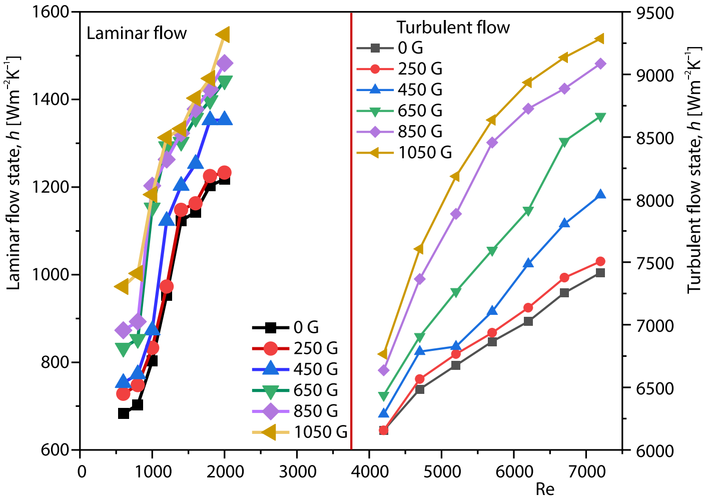

Figure 5. The relation among the CHT of Al_2O_3-water nanofluids and the magnetic field

ditions as MNF, nanofluids without an imposed magnetic field had CHT coefficients of 0.86%, 11.16%, 19.74%, 22.75%, and 28.33%, respectively. The magnetic field strengths, B, ranged from 250 G to 1050 G and the Reynolds number was 2000. For both low and high magnetic fields, the curves show an upward trend in figs. 5(b) and 5(a), and the rates of rise are identical. The statistical analysis in the follow-up multiple linear regression model benefits from this strong linear connection suggestion (MLR). A maximal Reynolds number of 7500 and $B = 250$ G, 450 G, 650 G, 850 G, and 1050 G result in CHT coefficients that are 0.99%, 8.47%, 17.24%, 23.10%, and 25.79% better, respectively, than nanofluids that do not contain a magnetic field.

When subjected to B, the nanoparticles in MNF are drawn to the pipe surface due to the effect of the field strength. They then migrate quickly to the copper pipe's surface, increasing the concentration of particles there and causing heat to condense on them. Ultimately, this causes a notable rise in the thermal conductivity of the area. However, when particles gather close to the pipe's surface, it increases friction there, which disrupts the flow pattern and the thermal boundary-layer, leading to even more localised CHT [22]. Because magnetic forces, not thermal ones, strongly affect magnetic nanoparticles, they clump together to create chains that are directed parallel to the applied field, further increasing the overall thermal conductivity. Pairs, triplets, or small chains of particles aligned with the external magnetic field demonstrate this [23].

Modelling with MLR

Figures 6 and 7 show the connection between MLR and the Al_2O_3-MNF in the pipe. According to the results, there is a straight line connecting the variables that affect the CHT coefficient. The multiple linear regression model can thus reliably forecast the CHT coefficient of the pipe. For both turbulent and laminar flows, 42 data sets are available, and the function is a CHT coefficient. There are a total of 84 sets of input variables involving magnetic field strength and Reynolds number, 35 sets of values for the CHT coefficient, and 70 sets of values for mass percentage and Reynolds number in the data model.

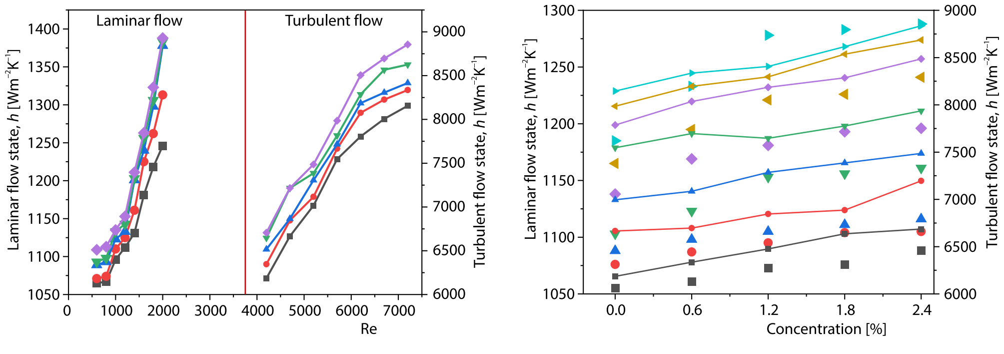

Figure 6. As independent variables, the Reynolds number and mass percentage are represented on the correlation graph

Multiple linear regression is used to fit the model for the CHT coefficient of the Al_2O_3-MNF in the pipe. The particle mass percentage, C, Reynolds number, h, and the CHT coefficient are the variables in this case with Reynolds number and mass percentage serving as the independent variables:

$$h = 0.1469\text{Re} + 26.1428C + 868.31 \tag{4}$$

$$h = 0.7053\mathrm{Re} + 278.3142C + 3262.69 \tag{5}$$

$$h = 0.4369\mathrm{Re} + 0.3313B + 344.26 \tag{6}$$

$$h = 0.6274\mathrm{Re} + 1.6695B + 3055.71 \tag{7}$$

Both the Reynolds number and the strength of the magnetic field are directly related to the eqs. (6) and (7). In order to evaluate and fine-tune particular fitting parameters for different techniques, the MLR findings are a great visual analysis tool. Researchers can gain a better grasp of the data and useful recommendations for improving ML model performance for more complicated datasets with non-linear interactions using this method. Although MLR cannot explicitly predict non-linear correlations, the aforementioned modelling does reveal close-to-linear interactions, which are useful for comparing with the two ML methods that follow.

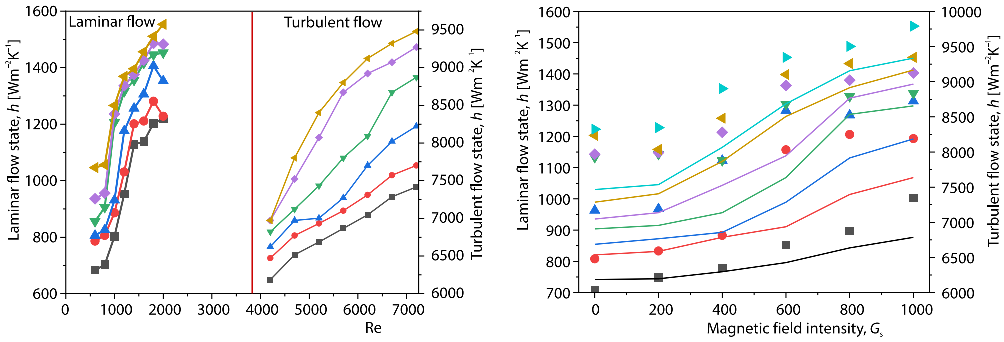

Figure 7. The correlation between the independent variables Reynolds number and magnetic field

Statistics with RB

The optimal MSE model for Al_2O_3-MNF was first determined using the grid searching cross validating technique with a invisible layer neuron count of 6, as part of the examination of RB models in ML techniques. The data model remains true to the original MLR for 86 sets and 75 sets, correspondingly, when 75% of the dataset is used for training and 25% for testing. All of the models were trained to be independent of the baseline weights and biases after 20 iterations, only the best findings from the ANN networks were shared. Particular comparisons of multi-parameter combinations are provided in the ML comparison section. These combinations include R^2, RMSE, MSE, AARD, and MAE [%].

The line plots in fig. 8(a) compare the actual values to the best-case scenario MSE simulation results following RB training. The CHT coefficient is the result, while the Reynolds number and mass percentage are the input variables. Comparing the simulation results with the actual data and input values of Reynolds number and B is revealed in fig. 8(b). The most accurate simulation results following RB training seem to deviate more from the real values than in fig. 8(a). The consequences of turbulent and laminar flows in a simulation, on the other hand, are very similar. The image clearly shows that the amount of sample data has less of an effect on the final simulation output and that fitted distortion is reduced. The data underfitting is minor in the turbulent flow scenario in particular.

The reliability of a model's predictions can be measured using the prediction accuracy diagram. Regression diagram for R^2 determination target utilising training data of fig. 8. A high degree of model accurateness is shown when the projected value is close to the true value and the expected point is close to the contour line. The results of the MSE performance are similar, but there is a larger data point deviation from the 45° line and smaller R^2 values for the turbulent and laminar flow phases.

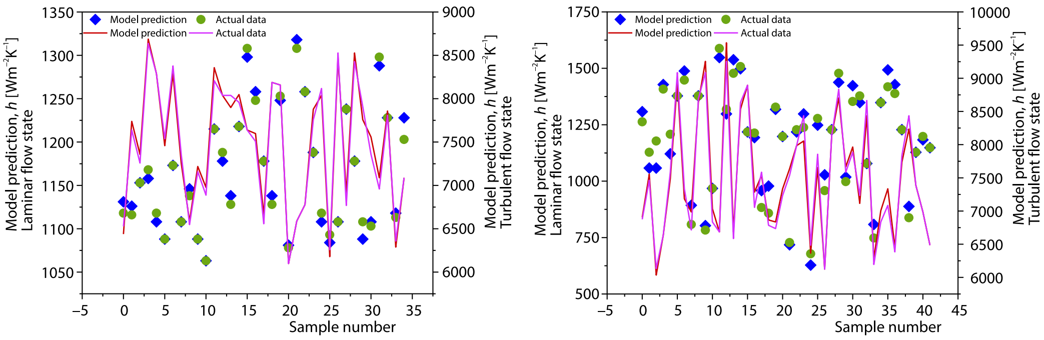

Figure 8. A comparison between the RB model's experimental results and its corresponding simulation deviation plot; (a) laminar flow state and (b) turbulent flow state

Conclusion

The CHT characteristics of Al_2O_3-water MNF in a pipe were thoroughly investigated by a thorough analysis that took both turbulent and laminar flow scenarios into account. The use of ML techniques to model the acquired data has never been attempted before. The CHT coefficient of Al_2O_3-MNF and its key affecting parameters were studied using a self-built platform. We used grid search cross-validation fit the results of RB, LS-SVM, and MLR in a sequential fashion. Using a battery of accuracy criteria, we pitted the RB and LS-SVM models against one another. In terms of overall performance, the LS-SVM model was better than the RB model. We visualised the expected and actual CHT coefficients of Al_2O_3-MNF in pipes using 3-D smoothed surface plots to validate and evaluate the model's accuracy. The LS-SVM model's validity and accuracy were further bolstered by these graphics. Statistical theory-based LS-SVM effectively addressed neural network issues and performed exceptionally well when forecasting very small amounts of data, according to the integrated research. The findings and recommendations of this work should be considered by ML researchers interested in MNF heat transfer performance in future studies.

References

[1] Zhang, Y., Xu, X., Machine Learning Specific Heat Capacities of Nanofluids Containing CuO and Al_2O_3, *AIChE Journal*, *67* (2021), 9

[2] Mukesh Kumar, P. C., Kavitha, R., Regression Analysis for Thermal Properties of Al_2O_3/H_2O Nanofluid Using Machine Learning Techniques, *Heliyon 6* (2020), 6

[3] Mackolil, J., Mahanthesh, B., Time-Dependent Non-Linear Convective Flow and Radiative Heat Transfer of Cu-Al_2O_3-H_2O Hybrid Nanoliquid with Polar Particles Suspension: a Statistical and Exact Analysis, *Bionanoscience*, *9* (2019), 4, pp. 937-951

[4] Chokkiyee, M. K. P., *et al*., Predictive Analysis of Heat Transfer Characteristics of Nanofluids in Helically Coiled Tube Heat Exchanger Using Regression Approach, *Thermal Science*, *24* (2020), 1B, pp. 505-513

[5] Adun, H., *et al*, An Experimental Investigation of Thermal Conductivity and Dynamic Viscosity of Al_2O_3--ZnO-Fe_3O_4 Ternary Hybrid Nanofluid and Development of Machine Learning Model, *Powder Technol*, *394* (2021), 4, pp. 1121-1140

[6] Mukesh Kumar, P. C., Kavitha, R., Prediction of Nanofluid Viscosity Using Multilayer Perceptron and Gaussian Process Regression, *Journal Therm. Anal. Calorim*., *144* (2021), 4, pp. 1151-1160

[7] Zhou, J., *et al*., Numerical Investigation, Environmental Consideration, and the Use of Machine Learning in Optimizing the Dimensions of a Rectangular Blade Between two Blades in the Presence of a Magnetic Field (Two-Phase Method), *Eng. Ana.l Bound Elem*., *149* (2023), Mar., pp. 71-85

[8] Saha G., aPaul, M. C., Analysis of Heat Transfer and Entropy Generation of TiO_2-Water Nanofluid-Flow in a Pipe under Transition, *Procedia Engineering*, *105* (2015), pp. 381-387
[9] Syah, R., *et al*., Numerical Investigation of Nanofluid-Flow Using CFD and Fuzzy-Based Particle Swarm Optimization, *Sci. Rep*., *11* (2021), 1
[10] Zhou, J., *et al*., Numerical Study of Mixed Convection Flow of Two-Phase Nanofluid in a 2-D cCvity with the Presence of A Magnetic Field By Changing the Height of Obstacles with Artificial Intelligence: Investigation of Entropy Production Changes and Bejan Number, *Eng. Anal Bound. Elem*., *148* (2023), Apr., pp. 52-61
[11] Shah, M. A., *et al.*, Use of Neural Network and Machine Learning in Optimizing Heat Transfer and Entropy Generated in a Cavity Filled Wwth Nanofluid under the Influence of Magnetic Field: A Numerical Study, *Eng. Anal. Bound. Elem*., *139* (2022), June, pp. 113-131
[12] Mesgarpour, M., *et al.*, An Investigation of the Thermal Behavior of Constructal Theory-Based Pore-Scale Porous Media by Using a Combination of Computational Fluid Dynamics and Machine Learning, *Int. J. Heat Mass Transf*., *194* (2022), 123072
[13] Ozgirgin Yapıcı, E., *et al*., Analysis of Heat Transfer Enhancement of Passive Methods in Tubes with Machine Learning, ARCHIVE Proceedings of the Institution of Mechanical Engineers, Part C, *Journal of Mechanical Engineering Science 1989-1996, 203-210*, 2023
[14] Jery, A. E., *et al*., Numerical Simulation and Artificial Neural Network Prediction of Hydrodynamic and Heat Transfer in a Geothermal Heat Exchanger to Obtain the Optimal Diameter of Tubes with the Lowest Entropy Using Water and Al_2O_3/Water Nanofluid, *Geothermics*, *107* (2023), 102605
[15] Alimoradi, H., *et al*., A Parametric Study of Subcooled Flow Boiling of Al_2O_3/Water Nanofluid Using Numerical Simulation and Artificial Neural Networks, *Nanoscale and Microscale Thermophysical Engineering*, *26* (2022), 2-3, pp. 129-159
[16] Zhang, R., *et al*., Experimental Investigation and Machine Learning Modelling of Heat Transfer Characteristics for Water Based Nanofluids Containing Magnetic Fe_3O_4 Nanoparticles, *Mater Today Commun*., *36* (2023), 106798
[17] Rahnama, Z., Ansarifar, G. R., Predicting and Optimizing the Thermal-Hydraulic, Natural Circulation, And Neutronics Parameters in the Nuscale Nuclear Reactor Using Nanofluid As a Coolant Via Machine Learning Methods through GA, PSO, and HPSOGA Algorithms, *Ann Nucl. Energy*, *161* (2021), 108375
[18] Sahebi, S. A. R., *et a*l., On the thermal Performance of Nanofluid over a Cylinder Within a Confined Channel: The Splitter Effect, *Case Studies in Thermal Engineering*, *49* (2023), 103275
[19] Ahmed, Z., *et al*., The Al_2O_3-CO_2 Nanofluid Transport Properties: A Molecular Dynamics Study and Machine Learning Predictive Modelling, *Heat Transfer Engineering*, *44* (2023), 19, pp. 1747-1761
[20] Shahsavar, A., *et al*., Investigation on Two-Phase Fluid Mixture Flow, Heat Transfer and Entropy Generation of a Non-Newtonian Water-CMC/CuO Nanofluid Inside a Twisted Tube wwith Variable Twist Pitch: Numerical and evolutionary Machine Learning Simulation, *Eng. Anal. Bound. Elem*., *140* (2022), July, pp. 322-337
[21] Girimurugan, R., *et al.*, Application of Deep Learning to the Prediction of Solar Irradiance through Missing Data, *International Journal of Photoenergy*, *2023* (2023), ID4717110
[22] Alghamdi, W., *et al*., Turbulence Modelling through Deep Learning an In-Depth Study of Wasserstein GAN, *Proceedings*, 4th Int. Conf. on Smart Elec. and Communication, Trichy, India
[23] Fuxi, S., *et al*., Artificial Neural Network Modelling to Examine Spring Turbulators Influence on Parabolic Solar Collector Effectiveness with Hybrid Nanofluids, *Eng. Anal Bound. Elem*., *143* (2022), Oct., pp. 442-456

Paper submitted: March 10, 2023
Paper revised: September 15, 2023
Paper accepted: October 21, 2023